Hydrol. Earth Syst. Sci. Discuss., 6, 2189–2246, 2009
www.hydrol-earth-syst-sci-discuss.net/6/2189/2009/

Hydrology and Earth System Sciences Discussions

Papers published in *Hydrology and Earth System Sciences Discussions* are under open-access review for the journal *Hydrology and Earth System Sciences*

Distributed modeling of land surface water and energy budgets in the inland Heihe river basin of China

Y. Jia[1], X. Ding[1], C. Qin[1,2,3], and H. Wang[1]

[1]Department of Water Resources, Institute of Water Resources and Hydropower Research (IWHR), Beijing, 100038, China
[2]International Institute for Geo-Information Science and Earth Observation (ITC), 7500AA Enschede, The Netherlands
[3]The Center for Clean Technology and Environmental Policy (CSTM), University of Twente, 7500AE Enschede, The Netherlands

Received: 28 January 2009 – Accepted: 13 February 2009 – Published: 12 March 2009

Correspondence to: Y. Jia (ywjia@yahoo.com)

Published by Copernicus Publications on behalf of the European Geosciences Union.

Abstract

A distributed model for simulating the land surface hydrological processes in the Heihe river basin was developed and validated on the basis of considering the physical mechanism of hydrological cycle and the artificial system of water utilization in the basin. Modeling approach of every component process was introduced from 2 aspects, i.e., hydrological cycle and energy cycle. The hydrological processes include evapotranspiration, infiltration, runoff, groundwater flow, interaction between groundwater and river water, overland flow, river flow and artificial cycle processes of water utilization. A simulation of 21 years from 1982 to 2002 was carried out after obtaining various input data and model parameters. The model was validated for both the simulation of monthly discharge process and that of daily discharge process. Water budgets, spatial and temporal variations of hydrological cycle components as well as energy cycle components in the upper and middle reach Heihe basin (36 728 km^2) were studied by using the distributed hydrological model. In addition, the model was further used to predict the water budgets under the future land surface change scenarios in the basin. The modeling results show: 1) in the upper reach watershed, the annual average evapotranspiration and runoff account for 63% and 37% of the annual precipitation, respectively, the snow melting runoff accounts for 19% of the total runoff and 41% of the direct runoff, and the groundwater storage has no obvious change; 2) in the middle reach basin, the annual average evapotranspiration is 52 mm more than the local annual precipitation, and the groundwater storage is of an obvious declining trend because of irrigation water consumption; 3) for the scenario of conservation forest construction in the upper reach basin, although the evapotranspiration from interception may increase, the soil evaporation may reduce at the same time, therefore the total evapotranspiration may not increase obviously; the measure of changing the farmland to animal husbandry land in the middle reach basin has obvious effects on decreasing evapotranspiration, increasing the discharge at Zhengyixia as well as decreasing the storage deficit.

HESSD

6, 2189–2246, 2009

1 Introduction

The study on hydrological cycle at the river basin scale is of great significance to solve resources and environmental issues, which provides an important scientific basis for the research of water resources, flood forecasting, water environment, as well as water ecology. With the changes of global environment and land surface, the hydrological cycle has been greatly changed. The traditional hydrological statistical methods and lumped hydrological models cannot meet the practical demand. Physically-based distributed hydrological simulation could profoundly analyze every component of water cycle process and their inter-relationship in a holistic manner, which can help understanding watershed runoff variation and water resources evolution trend in the changing environment, impacts on hydrological cycle from human activities, and hydrological prediction in ungauged basins (PUBs). Therefore, it is of great significance to research and develop distributed hydrological models (Abbott et al., 1986).

Since 1960s, especially 1980s, high-intensive human activities have destroyed the natural system in the Heihe river basin, and caused serious ecological and environmental problems, including reduction of flow discharged to downstream, gradual disappearance of some seasonal rivers and, degradation of forest and grassland, frequently occurring of dust storms, etc. Rational water resources allocation and effective regulation are urgently needed to realize the harmonization between human and natural system. It is urgently needed, for the practical demand of water resources assessment, allocation and regulation, to develop runoff forecasting models and study the hydrological cycle mechanism and water resource evolution rules in the Heihe river basin. Besides inland mountainous hydro-meteorology, snow melting, soil vegetation and frozen soil, frequent conversion between river water and groundwater, impacts from high-intensive human activities in the middle reach basin and ecological water demand in lower reach regions are also involved in the hydrological system in the Heihe river basin. This is a rather complicated "human-nature" interaction system.

Meaningful explorations on hydrological simulation in the Heihe river basin have been

conducted by many scholars and institutions (Cao et al., 2000; CAS-CAREERI, 2000; Kang et al., 2002; Xia et al., 2003; Huang et al., 2004; Zhang et al., 2005; Wu et al., 2005). A conceptual model for monthly runoff, HBV model was used to simulate mountainous runoff process by dividing the upper mountainous reaches into two basic landscape zones, including mountainous snow and frozen soil zone, and mountainous vegetation zone (Kang et al., 2002). Distributed Time Variant Gain Model (DTVGM) was developed according to rainfall-runoff nonlinear theory and conceptual simulation method, which was applied in the upper reach basin (Xia et al., 2003). Distributed hydrological model SWAT was applied to simulate the runoff by dividing the upper reach main river into 157 hydrological response units (HRU) (Huang et al., 2004). Simulation of groundwater was conducted in the middle reach basin (Zhang et al., 2005; Wu et al., 2005). Despite these researches have already achieved good results, the existing models are commonly conceptual–based or the adopted spatial and temporal steps are too large. They are difficult to give a detailed description on the physical mechanism of hydrological cycle and accompanied processes, and to effectively analyze the role of every hydrological component on the whole water cycle process, e.g. the spatial and temporal distributions of rainfall, topography, land surface, soil, geology and water consumption, etc. In addition, they are also difficult to predict water resources evolution trend under the impacts of future land surface change and human activity.

In this paper, the water and energy transfer processes (WEP) model (Jia et al., 2001, 2003) is applied and improved for the simulation of hydrological system in the Heihe river basin by adding simulation of snow melting process, as well as more detailed analysis on the anthropogenic water use processes. After calibration and validation, the improved model WEP-Heihe is used to research hydrological process and water/energy budgets and provides a basis for water resources assessment, allocation and management in the basin.

2 Model development

2.1 Model structure

The spatial calculation unit of WEP model is a square or rectangular grid. The vertical structure within a grid cell is shown in Fig. 1a, and the horizontal structure within a watershed is shown in Fig. 1b. Each grid cell in the vertical direction, from top to bottom, includes nine layers, namely an interception layer, a depression layer, three upper soil layers, a transition layer, an unconfined aquifer and two confined aquifers. State variables include depression storage on land surface and canopies, soil moisture content, land surface temperature, groundwater tables and water stages in rivers, etc. To consider the subgrid heterogeneity of land use, the mosaic method (Avissar and Pielke, 1989) is used which reflects composition of different land uses within a grid cell. The areal average of water and heat fluxes from all land uses in a grid cell produces the averaged fluxes in the grid cell. Land use is at first divided into three groups, namely a water body group, a soil-vegetation group and an impervious area group. The soil-vegetation group is further classified into bare soil, tall vegetation (forest or urban trees) and short vegetation (grass or crops). The impervious area group consists of impervious urban cover and urban canopy. In addition, for the convenience of describing soil evaporation, grass or crop root water uptake and tree root water uptake and reflecting surface soil moisture content change with changing root depth, the surface soil of soil-vegetation group is divided into 3 layers. Runoff routings on slopes and in rivers are carried out by applying one-dimensional kinematical wave approach from upstream to downstream. Numerical simulation of multilayered aquifers is performed for groundwater flows in mountainous and plain areas separately with the consideration of groundwater exchange with surface water, soil moisture and stream flow (Jia et al., 2003).

HESSD
6, 2189–2246, 2009

2.2 Hydrological processes

2.2.1 Evapotranspiration

Evapotranspiration in a grid cell consists of interception of vegetation canopies , evaporation from water body, soil, urban cover and urban canopy and transpiration from the dry fraction of leaves with the source from the three soil layers. The averaged evapotranspiration E is expressed as:

$$E = F_W E_W + F_{SV} E_{SV} + F_U E_U \quad (1)$$

Where F_W, F_{SV} and F_U are the area fractions of water body, soil-vegetation and impervious area, respectively, E_W, E_{SV} and E_U are the evaporation or evapotranspiration from them, respectively.

The evaporation from the water body group is calculated with the Penman equation:

$$E_W = \frac{(RN - G)\Delta + \rho_a C_P \delta_e / r_a}{\lambda(\Delta + \gamma)} \quad (2)$$

where RN is the net radiation, G is the heat conduction, Δ is the gradient of saturated vapour pressure to temperature, δ_e is the air vapour pressure deficit, r_a is the aerodynamic resistance, ρ_a is the air density, C_p is the air specific heat, λ is the latent heat of water and γ is the psychometric constant.

The evaporation from the impervious area group is taken as the smaller one of current depression storage and the potential evaporation. The maximum depression storage of impervious area is assumed as 2 mm in this study.

The evapotranspiration from the soil–vegetation group is calculated as follows:

$$E_{SV} = E_{i1} + E_{i2} + E_{tr1} + E_{tr2} + E_s \quad (3)$$

Where E_i is the interception of vegetation, E_{tr} is the transpiration from the dry part of vegetation leaves with numbers 1 and 2 representing tall vegetation and short vegetation, respectively and E_s is the evaporation from soils.

The computation of interception is referred to as the following model (Noilhan and Planton, 1989):

$$E_i = Veg \cdot \delta \cdot E_V \tag{4}$$

$$\partial W_r/\partial t = Veg \cdot P - E_i - R_r \tag{5}$$

$$R_r = \begin{cases} 0 & W_r \le W_{r\max} \\ W_r - W_{r\max} & W_r > W_{r\max} \end{cases} \tag{6}$$

$$\delta = (W_r/W_{r\max})^{2.3} \tag{7}$$

$$W_{r\max} = 0.2Veg \cdot LAI \tag{8}$$

Where Veg is the fraction of tall (or short) vegetation in the soil-vegetation group, δ is the fraction coefficient of the foliage covered by a water film, E_V is the potential evaporation on vegetation surface, W_r is the storage of the interception reservoir, $W_{r\max}$ is the maximum W_r (mm), P is the precipitation, R_r is the drainage rate from the canopy when W_r exceeds $W_{r\max}$ and LAI is the leaf area index.

The transpiration is expressed as:

$$E_{tr} = Veg \cdot (1 - \delta) \cdot E_{PM} \tag{9}$$

$$E_{PM} = \frac{(RN - G)\Delta + \rho_a C_P \delta_e / r_a}{\lambda \left[\Delta + \gamma(1 + r_c/r_a)\right]} \tag{10}$$

Where E_{PM} is the Penman–Monteith transpiration (Monteith, 1973), r_c is the canopy resistance and the others as denoted above.

The transpiration is actually supplied from soil layers by roots. A root uptake model is adopted which assumes that the root uptake intensity linearly decreases with the increase of root depth and the uptake in the upper half root zone accounts for 70% of the total uptake. The transpiration of tall vegetation is assumed to originate from the three upper soil layers in Fig. 1 while that of short vegetation from only the two upper ones.

The aerodynamic resistance and canopy resistance are two important parameters for the evapotranspiration calculation. In the model, the aerodynamic resistance under neutral atmospheric conditions is calculated according to turbulent diffusion theory; the Monin–Obukhov similarity theory is used to modify the computation of aerodynamic resistance under unstable and stable atmospheric conditions; the canopy resistance is calculated by the Dickinson equation (Dickinson et al., 1984).

Evaporation from soils is assumed to come only from the top layer. It is usually estimated by multiplying the potential evaporation (based on the Penman equation) with an evaporation coefficient, which is called the potential method hereafter. However, the potential method may cause theoretical inconsistency of heat flux partition on soil surface because the net radiation and soil heat flux corresponding to the saturated vapour pressure of soil are used in the Penman equation while the actual soil may be unsaturated. Based on the energy balance on the soil surface, aerodynamic diffusion equations of latent and sensible heat fluxes and the wetness function concept, we derived the following modified Penman equation to compute actual soil evaporation directly:

$$E_S = \frac{(RN - G)\Delta + \rho_a C_P \delta_e / r_a}{\lambda(\Delta + \gamma/\beta)} \tag{11}$$

Where β is the wetness function and the other notations are the same as mentioned above.

2.2.2 Infiltration

Considering infiltration into a vertical uniform soil column when the surface is ponded, Green and Ampt proposed an infiltration model by assuming there is a wetting front which separates saturated soil above from soil below and by using Darcy's law. Compared with the other infiltration models, the Green-Ampt model has the advantages of simplicity, physically-based characteristics and measurable parameters. Mein and Larson (1973) extended it to model infiltration into uniform soil during a steady rain and

Moore and Eigel (1981) extended it to model infiltration into two-layered soil profiles during steady rains.

Jia and Tamai (1997) suggested a generalized Green-Ampt model for infiltration into multilayered soil profiles during unsteady rains on the basis of Moore and Eigel (1981). The generalized Green-Ampt model is adopted in this study.

2.2.3 Surface runoff

In the water body group, surface runoff is estimated as precipitation minus evaporation. In the impervious area group, surface runoff can be obtained by doing balance analysis of depression storage, precipitation and evaporation on land surfaces.

In the soil-vegetation group, surface runoff consists of two parts, namely the infiltration excess (Hortan type runoff) during heavy rainfall periods and the saturation excess (Dunne-type runoff) during the other periods. A heavy rainfall period is defined as a period during which the rainfall intensity is larger than the saturated soil hydraulic conductivity.

The infiltration excess $R1_{ie}$ is solved by applying the generalized Green-Ampt model to infiltration in three soil layers during heavy rainfall periods. The equations to compute the infiltration excess are as follows:

$$\frac{\partial H_s}{\partial t} = P - E_0 - f - R1_{ie} \tag{12}$$

$$R1_{ie} = \begin{cases} 0 & H_s \le H_{s\max} \\ H_s - H_{s\max} & H_s > H_{s\max} \end{cases} \tag{13}$$

Where H_s is the depression storage on soil surface, $H_{s\max}$ is the maximum depression storage, P is the rainfall, E_0 is the evaporation, f is the infiltration rate calculated with the generalized Green-Ampt model. In Eq. (12), E_0 equals the potential evaporation and transpiration is neglected during heavy rainfall periods.

The saturation excess $R1_{ie}$ during the left periods may occur if the groundwater level in the unconfined aquifer rises and the top soil layer becomes nearly saturated. It is

deduced by doing balance analysis in every soil layer (the Richards model) as follows:

(1) Depression storage layer

$$\frac{\partial H_s}{\partial t} = P(1 - Veg_1 - Veg_2) + Veg_1 \cdot R_{r1} + Veg_2 \cdot R_{r2} - E_0 - Q_0 - R1_{se} \quad (14)$$

$$R1_{se} = \begin{cases} 0 & H_s \le H_{s\max} \\ H_s - H_{s\max} & H_s > H_{s\max} \end{cases} \quad (15)$$

(2) Top soil layer

$$\frac{\partial \theta_1}{\partial t} = \frac{1}{d_1}(Q_0 + QD_{12} - Q_1 - R2_1 - E_1 - E_{tr11} - E_{tr21}) \quad (16)$$

(3) Second soil layer

$$\frac{\partial \theta_2}{\partial t} = \frac{1}{d_2}(Q_1 + QD_{23} - QD_{12} - Q_2 - R2_2 - E_{tr12} - E_{tr22}) \quad (17)$$

(4) Third soil layer

$$\frac{\partial \theta_3}{\partial t} = \frac{1}{d_3}(Q_2 - QD_{23} - Q_3 - E_{tr13}) \quad (18)$$

$$Q_j = k_j(\theta_j) \quad (j = 1, 2, 3) \quad (19)$$

$$E_0 = \min\left\{E_p, (H_s + P_{in})E_p/(E_p + Q_p)\right\}; \quad E_1 = E_s - E_0;$$

$$P_{in} = P(1 - Veg_1 - Veg_2) + (Veg_1 R_{r1} + Veg_2 R_{r2}) \quad (20)$$

$$Q_0 = \min\left\{Q_p, (H_s + P_{in})Q_p/(E_p + Q_p)\right\};$$

$$Q_P = \min\left\{k_1(\theta_s), Q_{0\max}\right\}; \quad Q_{0\max} = W_{1\max} - W_{10} - Q_1 \quad (21)$$

$$QD_{j,j+1} = k_{j,j+1} \cdot \frac{\phi_j(\theta_j) - \phi_{j+1}(\theta_{j+1})}{(d_j + d_{j+1})/2};$$

$$k_{j,j+1} = \frac{d_j * k_j(\theta_j) + d_{j+1} * k_{j+1}(\theta_{j+1})}{d_j + d_{j+1}} (j = 1, 2) \quad (22)$$

In the above equations, H_s is the depression storage on soil surface, $H_{s\max}$ is the maximum H_s, Veg_1 and Veg_2 is the fraction of tall and short vegetation, respectively, R_{r1} and R_{r2} is the drainage rate from tall and short vegetation, respectively, Q is the gravity drainage, $QD_{j,j+1}$ is the suction diffusion from the $(j+1)$th soil layer to the jth layer, E_0 and E_1 is the evaporation from the depression storage layer and top soil layer, respectively, E_{tr} is the transpiration with the first subscript representing vegetation type (1=tall vegetation and 2=short vegetation) and the second one representing soil layer, R_2 is the subsurface runoff, θ is the moisture content, θ_s is the saturated moisture content, $k(\theta)$ is the hydraulic conductivity correspondent to θ, $\phi(\theta)$ is the soil suction correspondent to θ, d is the thickness of the soil layer, $W=\theta d$ is the water storage of the soil layer, W_{10} is the initial water storage of the top soil layer and the other notations are the same as mentioned above. Except where especially mentioned, the numbers or subscripts of all variables mean layer numbers with 0, 1, 2 and 3 representing depression storage layer, top soil layer, second soil layer and third soil layer, respectively.

The continuity of water movement is considered when the application of the generalized Green-Ampt model is switched into that of the Richards model and vice versa. When the application of the generalized Green-Ampt model is switched into that of the Richards model, the initial moisture contents of three unsaturated soil layers for the Richards model are computed based on the depth of the wetting front from the generalized Green-Ampt model. However, when the application of the Richards model is switched into that of the generalized Green-Ampt model, the moisture contents of the three soil layers from the Richards model provide initial values for the generalized Green-Ampt model and no special treatment is required.

HESSD
6, 2189–2246, 2009

2.2.4 Subsurface runoff

The subsurface runoff is calculated according to the land slope and the soil hydraulic conductivity:

$$R2 = k(\theta)\sin(slope)L\,d \tag{23}$$

Where $R2$ is the subsurface runoff from the unsaturated soil layers, L is the channel length in the grid and the others as denoted above.

2.2.5 Groundwater flow and groundwater outflow

Taking account of the recharge from unsaturated soil layers and lifted groundwater as source terms, a two-dimensional numerical simulation of multilayered aquifers is performed for groundwater flow to consider the interactions between surface water and groundwater by using the following Boussinesq equations (Zaradny,1993):

Unconfined aquifer:

$$C_u\frac{\partial h_u}{\partial t} = \frac{\partial}{\partial t}\left(k_u h_u\frac{\partial h_u}{\partial x}\right) + \frac{\partial}{\partial y}\left(k_u h_u\frac{\partial h_u}{\partial y}\right) + (Q_3 + WUL - RG - Per - E) \tag{24}$$

Confined aquifer:

$$C\frac{\partial h}{\partial t} = \frac{\partial}{\partial x}\left(kD\frac{\partial h}{\partial x}\right) + \frac{\partial}{\partial y}\left(kD\frac{\partial h}{\partial y}\right) + (Per - GWP - Perc) \tag{25}$$

Where C_u is the specific yield, C is the storage coefficient, h_u and h is the groundwater heads in the unconfined aquifer and confined aquifers, respectively, k_u and k is the hydraulic conductivities of the unconfined aquifer and confined aquifers, respectively, D is the thickness of confined aquifers, Q_3 is the recharge from unsaturated soil layers, RG is the groundwater outflow to rivers, WUL is the water use leakage, GWP is the pumped groundwater, Per and $Perc$ is the percolation to the aquifer below and E is the evapotranspiration from groundwater when the unconfined groundwater level

rises above the third soil layer in Fig. 1a. $E=F_{SV}E_{tr13}$ if h_u rises to the third soil layer, $E=F_{SV}(E_{tr12}+E_{tr13}+E_{tr22})$ if h_u rises to the second soil layer or if h_u rises to the top soil layer with the notations as described above.

Groundwater outflow is calculated according to the hydraulic conductivity k_b of riverbed material and the difference between river water stage H_r and groundwater level h_u:

$$RG = \begin{cases} k_b A_b (h_u - H_r)/d_b & h_u \geq H_r \\ -k_b A_b [1 + (H_r - Z_b)/d_b] & h_u < H_r \end{cases} \quad (26)$$

Where A_b is the seepage area of the riverbed, Z_b is the elevation of the riverbed and d_b is the thickness of the riverbed material.

2.2.6 River flow and overland flow

The river flow and overland flow are routed by using the kinematic wave method:

$$\frac{\partial A}{\partial t} + \frac{\partial Q}{\partial x} = q_L \quad (27)$$

$$Q = \frac{A}{n} R^{2/3} S_0^{1/2} \quad (28)$$

Where A is the area of lateral section, Q is the discharge, q_L is the lateral inflow of unit channel length, n is the Manning roughness, R is the hydraulic radius, S_0 is the longitudinal slope of the river bed.

2.2.7 Snow melting process and frozen soil consideration

Although energy balance method provides a good physical basis for describing snow melting process, simple and practical Temperature-index approach is used to simulate daily or monthly snow melting process since too many parameters and data are needed to solve energy balance equation. In this study, the Temperature-index approach is

adopted:

$$SM = M_f(T_a - T_0) \tag{29}$$

$$\frac{dS}{dt} = SW - SM - E \tag{30}$$

Where SM is the snow melting amount (mm/day), M_f is the melting coefficient (mm/°C/day), T_a is the temperature index (°C), T_0 is the critical melting temperature (°C), S is the water amount transfered from the snow (mm), SW is the water amount transfered from the snowfall (mm), E is the sublimation amount from the snow (mm).

The melting coefficient is generally considered as a model debugging parameter since it changes with elevation and seasons as well as land surface conditions changed. The value is usually 1~7 mm/°C/day. The value of bare soil is larger than that of grass land, while the latterr is larger than that of forest. Daily average temperature is usually selected as the temperature index. The critical melting temperature is usually −3~0°C. In addition, rain-snow critical temperature parameter is needed to distinguish rainfall and snowfall (usually 0~3°C).

The temperature influence to the saturated hydraulic conductivity in the frozen soil is computed as:

$$k_f = \begin{cases} K_0 & T_a \geq T_c \\ k_0 e^{aT_a+b} & T_a < T_c \end{cases} \tag{31}$$

Where k_f is the saturated hydraulic conduction coefficient; k_0 is the saturated hydraulic conduction coefficient when frozen earth melt; T_a is the average daily temperature; T_c is the critical temperature of melting; a, b are constants. Through model calibration based on the observed river base flow, it is found that T_c=−5°C, a=0.05, and b=0.25 in the Heihe basin.

2.2.8 Anthropogenic components

The water use in every grid is deduced by using population and water use per capita. The water use per capita is decided according to statistics of water use in a watershed.

In addition, water use leakage is deduced from water use and the leakage rate of water supply system. The sewerage is equal to water use subtracted by leakage, and it is set as one part of the lateral inflow to the channel.

The groundwater lift is divided into the domestic water, industrial water and the irrigation water. The domestic water is calculated according to the annual regional domestic water lift and the population distribution, and the industrial water is deduced based on the GDP distribution. The irrigation water is calculated based on the annual lift, irrigation area and irrigation rule.

2.3 Energy processes

The energy balance equation on land surface is expressed as:

$$RN + Ae = lE + H + G \tag{32}$$

$$RN = RSN + RLN \tag{33}$$

Where RN is the net radiation, Ae is the anthropogenic energy source, lE is the latent heat flux, H is the sensible heat flux, G is the heat conduction into soil, RSN is the net short-wave radiation and RLN is the net long-wave radiation.

2.3.1 Short-wave radiation

Because of unavailability of the direct observation data of the incoming short-wave radiation, it is estimated from the sunshine hours Based on Shimazaki (1996). It at first deduces the direct short-wave radiation and the diffusion short-wave radiation based on the sunshine levels in current and prior hours, and then adds them up to obtain the total short-wave radiation after considering the solar zenith angle. The net short-wave radiation on each land use is as follows after considering the albedo and the sheltering factors.

(1) Water body

$$RSN_W = RS(1 - \alpha_W) \tag{34}$$

(2) Soil-vegetation group Soil:

$$RSN_S = RS(1-\alpha_S)(F_{\text{soil}} + \tau_1 \cdot Veg_1 + \tau_2 \cdot Veg_2) \quad (35)$$

Tall vegetation:

$$RSN_{V1} = RS(1-\alpha_{V1})Veg_1 - RS(1-\alpha_S)\tau_1 \cdot Veg_1 \quad (36)$$

Short vegetation:

$$RSN_{V2} = RS(1-\alpha_{V2})Veg_2 - RS(1-\alpha_S)\tau_2 \cdot Veg_2 \quad (37)$$

$$\tau_1 = \exp(-0.5LAI_1)\tau_2 = \exp(-0.5LAI_2) \quad (38)$$

(3) Impervious group
Urban cover:

$$RSN_{U1} = RS(1-\alpha_{U1})F_r\beta \quad (39)$$

Urban canopy:

$$RSN_{U2} = RS(1-\alpha_{U2})F_r\beta \quad (40)$$

where RSN is the net short-wave radiation, α is the albedo, τ_1 is the transmission of short-wave radiation of tall vegetation, τ_2 is the transmission of short-wave radiation of short vegetation, F_{soil}, Veg_1 and Veg_2 are the area fractions of bare soil, tall vegetation and short vegetation in the soil-vegetation group, respectively, LAI is the leaf area index, F_r is the area fraction of urban cover in the impervious area group, β is the sky view factor of urban cover. Subscripts *W, S, V1, V2, U1 and U2* denote water body, bare soil, tall vegetation, short vegetation, urban cover and urban canopy, respectively.

2.3.2 Long-wave radiation

The long-wave radiation is calculated by following Kondo (1994) who separately deduce the downward long-wave radiation from atmosphere to landsurface and the upward

long-wave radiation from landsurface to atmosphere based on the air temperature and the landsurface temperature. Net long-wave radiation is equal to the downward long-wave radiation subtracted by the upward one. Its expression for each land use is as follows:

(1) Water body

$$RLN_W = RLD - RLU_W \tag{41}$$

(2) Soil-vegetation group

Soil:

$$RLN_S = (RLD - RLU_S)F_{\text{soil}} + (RLU_{V1} - RLU_S)Veg_1 + (RLU_{V2} - RLU_S)Veg_2 \tag{42}$$

Tall vegetation:

$$RLN_{V1} = (RLD + RLU_S - 2RLU_{V1})Veg_1 \tag{43}$$

Short vegetation:

$$RLN_{V2} = (RLD + RLU_S - 2RLU_{V2})Veg_2 \tag{44}$$

(3) Impervious group

Urban cover:

$$RLN_{U1} = [RLD\beta - RLU_{U1} + RLU_{U2}(1-\beta)] + RLU_{U1}F_r(1-\beta) \tag{45}$$

Urban canopy:

$$RLN_{U2} = RLD(1 - F_r\beta) - RLU_{U2}[1 - F_r + 2F_r(1-\beta)] + RLU_{U1}F_r(1-\beta) \tag{46}$$

Where the notations are the same as described above.

2.3.3 Antropogenic energy consumption

Statistic energy consumption indices on various types of urban land use are used to consider the impact of human activities on energy balance in an urban area (Kawamata,1994). Half of the energy consumption is assumed to emit to land surfaces and the other half to the air.

2.3.4 Latent heat flux

In the hydrological processes part, the computation of evapotranspiration has been described in details. The latent heat flux λE can be obtained by multiplying the evapotranspirationwith the latent heat of the water λ.

2.3.5 Sensible heat flux

The sensible heat flux H can be expressed as:

$$H = \rho_a C_P (T_s - T)/r_a \tag{47}$$

where ρ_a is the density of the air, C_P is the specific heat of the air, T is the air temperature, T_s is the surface temperature and r_a is the aerodynamic resistance.

2.3.6 Heat conduction into soil

Based on the energy balance equation we get:

$$G = (RN + Ae) - (\lambda E + H) \tag{48}$$

2.3.7 Surface temperature

The force-restore method (FRM) is used to solve the surface temperature of different land covers. Hu and Islam (1995) suggested an optimal parameter α, which not only ensure minimum distortion of FRM to sinusoidal diurnal forcing but also makes distortion to higher harmonics negligible. They are followed in this research with the equations as follows:

$$\alpha \frac{\partial T_s}{\partial t} = \frac{2}{c_h \cdot d_0} G - \omega (T_s - T_d) \tag{49}$$

$$\frac{\partial T_d}{\partial t} = \frac{1}{\tau} (T_s - T_d) \tag{50}$$

$$\alpha = 1 + 0.943\left(\frac{\delta}{d_0}\right) + 0.223\left(\frac{\delta}{d_0}\right)^2 + 0.0618\left(\frac{\delta}{d_0}\right)^3 - 0.00527\left(\frac{\delta}{d_0}\right)^4 \quad (51)$$

$$d_0 = \sqrt{2k_h/(c_h\omega)} \quad (52)$$

where G is the heat conduction into soil, T_s is the surface temperature, T_d is the deep soil temperature (approximated as the daily average of T_s), δ is the considered soil depth (selected as the thickness of top soil layer), d_0 is the damping depth of the diurnal temperature wave, k_h is the soil heat conductivity, c_h is the soil volumetric heat capacity, $\omega=2\pi/\tau$ and τ=86 400. The soil thermal properties depend on the water content and the mineral composition of the soil. The soil heat capacity c_h and the soil heat conductivity k_h are referred to Kondo (1994).

3 Model calibration and validation

3.1 Input data preparation

The distribution of the rivers and main hydro-meteorological stations in upper and middle reaches of the Heihe river basin is shown in Fig. 2. The rivers in the basin include mainstream of the Heihe river, east branch Babao river in the upper reach, Liyuan river in the middle reach and several small rivers in mountainous areas. For model validation, geographic data including geological features, soil vegetation, hydrological and meteorological data and land use data as well as relevant socio-economic data (population and GDP for every county in 1981–2002) and water use data (in 1981–2002 for every county and irrigation area) in the basin are collected and packed up in the GIS platform for use.

Based on the DEM of 1:25 000, basic geographic information such as elevation/topography (Fig. 3), slope and overland flow direction are obtained, and the basin is further divided into sub-basins on the basis of stream links deduced from the DEM

and observed river information. On the basis of the aforementioned geographic information, flow accumulation is calculated for flow routing calculation. The river section is divided combining with water diversion channels and control stations, and basic information including river length, gradient, top width and bottom width can be obtained. The upper and middle reaches of the Heihe river basin are divided into 6 sub-basins (as shown in Fig. 2) and 70 river sections. Limited to the river channel data, in this study, the river flow routings are only performed for the Heihe mainstream, Babao river and Liyuan river while the river flow routings for other tributaries and mountainous rivers are approximated as overland flow routings in the upper reach watershed. It is noticed that in the flat middle reach basin down Yingluoxia, due to less precipitation, stronger evaporation capacity and soil infiltration capacity, there is little surface runoff generated. Moreover, most river channels disappear in lower reaches due to irrigation water withdraw in the middle reach. Therefore, to simplify the calculation, except keeping the flow routing calculation for the Heihe river mainstream, overland flow routing calculation for the flat middle reaches is omitted in the study, but the cumulative surface runoff is considered as a lateral inflow of the mainstream.

The meteorological data used in the model include daily rainfall (snowfall), temperature, wind speed, sun-shine, humidity and maximum evaporation from 1981 to 2002 at 9 meteorological stations within or near the upper and middle reaches of the Heihe river basin: Gaotai, Zhangye, Yeniugou, Qilian, Shandan, Tuole, Jinta, Dingxin and Jiuquan (see Fig. 2). The hydrological data used in the model include precipitation, water level and discharge at 11 hydrological stations, among which five stations, Zhamashike, Qilian, Yingluoxia, Gaoya and Zhengyixia, are located at the main river of the Heihe river, two stations, Liyuanbao and Gangoumen, are located at Liyuan river (see Fig. 2). Monthly discharge data from 1981 to 2002 as well as daily discharge data from 1990 to 2002 are collected. The Thiessen method is used to estimate the meteorological data for each grid, however, the elevation effects on rainfall and air temperature are considered. Based on the correlation analysis of the elevation and the annual average daily values (1981–2002) of meteorological factors, it is found that air temperature

and rainfall have close correlations with the elevation (R^2=0.983 and 0.850, respectively) while sunshine hours, wind speed and relative humidity have low correlation coefficients (R^2=0.586, 0.002 and 0.381, respectively). Therefore, for every grid cell in the Thiessen polygon controlled by a meteorology gauge station, its air temperature is revised based on a lapse rate of −0.00546°C/m and the difference of its elevation from the gauge station elevation. The rainfall is also revised in a similar way though it increases with the elevation increase, while the elevation effects on the remaining meteorological factors are neglected. Figure 4 shows the distribution of total precipitation in 2000 in the upper and middle reach basin deduced in the aforementioned approach.

The land use data are based on the TM image data for 1985, 1995 and 2000, and further merged to 8 categories, water body, tall vegetation (forests and shrubs), short vegetation (grass and crops), bare land, impervious area and buildings, taking grid as basic units and the area percentage of each category in each grid is calculated. Figure 5 shows the land use distribution in 2000 as an example. The area percentage of each category in each grid in other years from 1981 to 2002 is obtained by linear interpolation method based on that of 1985, 1995 and 2000. The soil type is generalized into 3 types, sand, loam and clay. The aquifer thickness of Zhangye Basin in the middle reach is deduced from the geological survey data. The thickness of soil layer in the upper mountainous reaches of Yingluoxia as well as Liyuanhe Baisn is calculated in accordance with the law of diminishing exponentially with the distance from the valley, and the thickness of soil layer in the other regions is set as 2 m.

For 37 irrigation areas having detailed annual water use data (1981–2002), the spatial interpolation of water use (including woodland and grassland irrigation water use) is conducted according to irrigation area distribution and the water use data and is further distributed to the time scale of 10 days according to precipitation, cropping pattern and irrigation rules. For the other irrigation areas, the irrigation quota is set as 7500 m^3/ha. The domestic water use in every grid is deduced from the distribution of population and daily water use capita. Urban domestic water use quota for current level is 140 l/d, while rural is 50 l/d. The population in every grid is deduced from the county population

in the GIS platform.

3.2 Parameter estimation

The main parameters in the model include soil parameters, groundwater aquifer hydraulic conductivity and specific yield, vegetation parameters, roughness of overland and river channel and infiltration coefficient of river bed. Most parameters in the model are not needed to be calibrated, but for several important parameters including saturated soil hydraulic conductivity, groundwater aquifer hydraulic conductivity and specific yield, infiltration coefficient and thickness of river bed as well as the Manning roughness, some adjustments are conducted comparing simulated discharge with observed values during selected calibration period.

3.2.1 Soil

On the base of the soil moisture movement experimental research results in the Heihe river basin and adjacent regions (Wang et al., 2002; Zhu et al., 2002; Cong et al., 2005), soil moisture characteristics parameters are calculated (Table 1).

Meanwhile, according to the soil composition and soil moisture content, empirical formula is established to consider the change of soil thermodynamic properties parameters with soil humidity changing.

3.2.2 Groundwater aquifer

Groundwater aquifer hydraulic conductivity and specific yield in the Zhangye Basin are deduced using geological exploration data and groundwater simulation results. Mountainous aquifer parameters are deduced by combining with discharge simulation results, the saturated hydraulic conductivity is set as 65.5 m/month, and the specific yield is set as 0.05.

3.2.3 Vegetation

Vegetation parameters change with seasons. Main parameters of four vegetation types include vegetation coverage rate (veg), leaf area index (LAI), vegetation height (hc), root depth (lr) and minimum lobular impedance ($rsmin$). The monthly change of vegetation parameters is considered in the model.

3.2.4 Flow routing parameters

Manning roughness used in river flow routing calculation is deduced according to the National Hydrological Yearbook of China, while the Manning roughness used in overland flow routing calculation is deduced from the Manning roughness of every land use in the grid. After model adjustment, the Manning roughness of woodland, grassland, farmland, bare land and urban surface, water body is set as 0.3, 0.1, 0.05, 0.02 and 0.01, respectively. The exchange amount between surface river and groundwater is closely related to riverbed material properties. In this study, riverbed material thickness divided by riverbed material infiltration coefficient is established as the model debugging parameter. The final value is set as 1.0E-05/s for mountainous rivers and 2.5E-05/s for plain rivers.

3.2.5 Snow melting parameters

The snow melting coefficient and the melting critical temperature are also model debugging parameters. After model adjustment, the snow melting coefficient is set as 1 mm/°C/day for woodland, 2 mm/°C/day for grassland, 2 mm/°C/day for bare land, 5 mm/°C/day for urban land use and 1 mm/°C/day for glacier, respectively; the melting critical temperature is set as 0°C; the rain-snow critical temperature is set as 1°C.

3.3 Model validation

In the model calibration, the upper and middle reaches are divided into 36728 units by the square grid cell of 1 km×1 km, and a simulation from 1981 to 2002 is performed with a time step of day. The model is calibrated using daily and monthly discharge processes observed at Yingluoxia hydrological station from 1996 to 2000. The main calibration parameters include the saturated soil moisture hydraulic conductivity, the groundwater aquifer hydraulic conductivity and the specific yield, the infiltration coefficient of riverbed material and the Manning roughness of river and overland flows. Calibration rules include: (1) minimizing the average annual discharge error during the simulation period; (2) maximizing the Nash-Sutcliffe efficiency coefficient; (3) maximizing the correlation coefficient between simulated discharge and observed values.

Like other physically-based distributed hydrological models (such as SHE), the model calibration and parameter adjustment is conducted using the "trial and error" method, that is, firstly determine the initial value according to physical properties, experimental data and reference data, then adjust the parameters according to the above three rules. Specifically, the saturated hydraulic conductivity is adjusted according to soil types since it is sensitive to the total discharge amount and the peak discharge, then the aquifer hydraulic conductivity, the specific yield and the riverbed infiltration coefficient are adjusted according to soil types since they mainly affect total annual runoff and runoff in withdraw periods; the Manning roughness used in overland flow routing calculation is adjusted according to different land uses since it mainly affects the shape of flood peak in the discharge process curve. In addition, the snow melting coefficient and the melting critical temperature have great influence on summer discharge and rising time, the frozen soil hydraulic conductivity has great influence on dry season discharge in winter, so they are also adjusted according to discharge hydrograph.

After model calibration, keeping all model parameters unchanged, a continuous daily simulation of 22 years is performed. There are two model validation periods for monthly discharge process, Period 1: 1982 to 1995, and Period 2: 2001 to 2002; due to the

lack of observed data during 1982 to 1989, the two model validation periods for daily discharge process are: Period 1: 1990 to 1995, and Period 2: 2001 to 2002.

3.3.1 Monthly discharge process

The monthly discharge process at the Yingluoxia hydrological station in the upper reaches of the Herihe River Basin is well simulated with a high accuracy (Fig. 6). The simulation results are shown in Table 2. It can be found that the model is well validated in the two validation periods based on the relative error of annual average discharge, the Nash -Sutcliffe efficiency coefficient and the correlation coefficient.

Although the monthly discharge processes at other hydrological stations such as Zhamashike are not used to calibrate the model, the comparison of simulated results with observed values is conducted, which shows that the simulation results are close to the observed values (Fig. 7).

3.3.2 Daily average discharge process

The comparison of simulated daily discharge processes with observed values at the Yingluoxia hydrological station is shown in Fig. 5, the simulation results are shown in Table 3. From Fig. 8 and Table 3 we can find that the model is well validated in the two validation periods. Meanwhile, it is also found that the simulation accuracy of daily discharge process is lower than that of monthly discharge process. This is because: 1) the precipitation data at the daily scale are more spatial-temporally variable than those at the monthly scale, so the shorter time scale, the more obvious deviation between the spatial precipitation data obtained by spatial interpolation method and the actual observed values. This deviation will be possibly passed to the simulation of discharge process, thus the simulation accuracy at daily scale will be lower than that at monthly scale; 2) the actual dynamic mechanism of basin hydrological cycle is very complex, the mathematics description of the mechanism and method dissolving the spatial variety of land surface and soil properties value in the model could be further improved.

However, it is necessary to perform long time series of hydrological simulation at daily or even shorter time scale, the reasons are not only for the need of predicting daily discharge process, but also for the need of predicting future land surface and climate change impacts, which is determined by the dynamic mechanism of hydrological cycle and accompanied processes.

4 Model application

4.1 Spatial and temporal variations of hydrological and energy processes

A continuous simulation from 1981 to 2002 is performed with a grid size of 1 km and a time step of 1 day using the distributed hydrological model WEP-HeiHe to study detailed processes of water budgets and hydrological cycle components. As an example, the water budget of 1999 in the upper reach watershed (with an area of 9999 km^2) is shown in Fig. 9. From the figure we can see that the average evaporation in 1999 in the region is 258 mm, 123 mm of it comes from land surface and vegetation interception, and 135 mm of it comes from soil evaporation and vegetation transpiration; among the total 156 mm runoff, surface runoff, subsurface runoff and groundwater flow accounts for 70 mm, 24 mm and 62 mm, respectively, and about 2 mm of the total runoff is taken by farmland irrigation. According to the observed data at the Yingluoxia hydrological station, the runoff amount in 1999 is 1610 million m^3, which amounts to 161 mm runoff depth, while the simulated annual runoff depth is 154 mm, the relative error is 4.4%.

The daily simulation results show that, in the upper reach watershed, the annual average evapotranspiration and runoff during the period from 1982 to 2002 accounts for 63% and 37% of the annual precipitation (428 mm), respectively. 47% of mountainous runoff directly comes from surface runoff, and the other 53% comes from mountainous subsurface runoff and groundwater flow. The snow melting runoff accounts for 19% of the total runoff and 41% of the direct runoff. It should be noted that the snow melting runoff here include all the surface runoff when rain falls as snow, not only glacier melting

HESSD
6, 2189–2246, 2009

runoff.

From the view of annual variation, the evaporation and runoff in upper reaches increases as precipitation increases, but the increase rate of evaporation is less than that of runoff; storage change reflects the objective laws of water storage in flood years and water assumption in drought years (Fig. 10a). In the middle reach basin (with an area of 19 014 km^2 not including the Liyuan river basin), the annual average evapotranspiration is 52 mm more than the local annual precipitation (240 mm), which amounts to 990 million m^3. This is due to the great amount of farmland irrigation water consumption in the middle reach Zhangye Basin and Shandan–Minle Plain. The deficit generally equals to the difference between the upper reach inflow and the outflow at Zhengyixia (Fig. 10b).

The distribution of actual evapotranspiration, surface runoff, groundwater outflow and sensible heat flux in the upper and middle reach basin in 2000 is shown in Fig. 11. From the figure we can see that, surface runoff mainly generates in upper mountainous reaches, runoff in valleys and low-lying areas mostly come from the groundwater outflow from soil layers in mountainous areas. There is nearly no runoff generated in the lower reach basin except Linze low-lying areas and bare rock regions. Groundwater is recharged by river water seepage from Yingluoxia to Zhangye, while groundwater overflows to river from Zhangye to Zhengyixia. In addition, the distribution of evapotranspiration shows that the Zhangye Basin, the Minle-Shandan irrigation areas as well as artificial oases are the main evapotranspiration zones.

Unsaturated soil is divided into 3 layers and moisture content in each layer is calculated in detail in the WEP-HeiHe model, so the distribution of moisture content in simulation periods could be obtained. As an example, the spatial distribution of surface soil moisture content in 1 March 2000 and 1 May 2000 is shown in Fig. 12. From the figure we can see the spatial variation of soil moisture content and the agricultural irrigation impacts in the middle reach basin. Snow is the important water information in dry seasons especially during planting and distributing water period in spring. The model developed in this study can be used to calculate the distribution of snow at

the beginning of calculation period and predict the distribution of snow at the end of calculation period (Fig. 13). Groundwater level is the important water information for integrated groundwater-surface water regulation in the middle reach basin. The model can be used to calculate the distribution of groundwater level at the beginning of calculation period and predict the distribution of groundwater level at the end of calculation period (Fig. 14). In addition, the model can be used to calculate the distribution of each element in energy processes including surface temperature (Fig. 15), sensible heat flux (Fig. 16), long-wave radiation (Fig. 17), short-wave radiation (Fig. 18), net radiation (Fig. 19) and the heat conduction into soil (Fig. 20).

Although the distributions of soil moisture content, groundwater level and snow simulated by the model look like reflecting the actual conditions of topography, hydrometeorology and agricultural irrigation, the simulation results have not been validated limited to data obtained. In the future, ground and remote sensing observed data will be used to validate the simulation results in order to support basin water resources management.

4.2 Water budgets prediction under the future land surface change

The distributed hydrological model developed in the study is based on the hydrological mechanism of the Northwest inland basin of China. The model parameters can be deduced from the physical properties of land surface and do not change with the changing precipitation. Therefore, the model may be used to predict the water budgets and water resources under the future land surface change, and to conduct scenario analysis under continuous deteriorated conditions and estimate the effects of adopting countermeasures.

4.2.1 Impacts of conservation forest construction in the upper reach basin

Assuming that the land covered with few woods in the upper reach basin with an area of 249.6 km^2 is all changed to forest, using the conditions of precipitation and meteo-

rology in 1999, the effects on water budgets in the upper reach basin simulated by the model are shown in Table 4. The simulation results show that, due to the construction of conservation forest in the upper reach basin, although the evapotranspiration from interception increases, the soil evaporation reduces at the same time, therefore the total evapotranspiration does not increase obviously; the runoff outflow slightly decreases, while the storage variable of soil moisture and groundwater slightly increase mitigating the deficit of storage variable in drought years such as 1999. It should be noted that the more important effects of conservation forest construction are to preserve the soil and water, decrease soil erosion in the upper reach and avoid sand sedimentation in the lower reach, thus improve the ecological environment in the basin.

4.2.2 Impacts of changing farmland to animal husbandry land in the middle reach basin

Assuming that 20% of the farmland with an area of 0.37 million hectares in the middle reach in current level is changed to animal husbandry land, using the conditions of precipitation and meteorology in 1999, the effects on water budgets in the middle reach basin simulated by the model are shown in Table 5. It can be seen that, due to the measure of changing the farmland to animal husbandry land in the middle reach basin, irrigation water consumption is greatly reduced, evapotranspiration and the storage variable deficit decreases obviously, while the discharge at Zhengyixia increases obviously. Therefore, the measure is urgently needed in the inland basin with serious water shortage problems.

5 Conclusions

In this study, a physically and GIS based distributed hydrological model was developed in the Heihe river basin. A simulation of 22 years was carried out with a grid size of 1km and a time step of 1 day in the upper and middle reach basin, and the model was vali-

dated using observed runoff data. The validation results show that the model has high simulation accuracy. The characteristics of the model are listed as following: (1) different from the existing methods of runoff simulating and flow routing, the model simulates all the processes during hydrological cycle, and couples the simulation of hydrological cycle process with energy cycle process; (2) to consider the subgrid heterogeneity of land use within a calculation unit, the mosaic method is used by dividing the land use into 8 categories, and water and heat fluxes for each land use is calculated separately, thus greatly improve the calculation accuracy using large grids in large basin, while only one dominant type of land use is considered in most of the existing models; (3) the model developed in the study has a quick calculation speed (the calculation time is about 15 min for 1-year simulation of 36728 grid units in the upper and middle reach of the Heihe river basin using a PC computer with CPU 2.2 GHz). In addition, the parameters in the model are all physically-based and can be measured or deduced, and the model was well validated. Therefore, the model has the potential to be applied to PUBs.

The results of applying the distributed hydrological model to the upper and middle reach of the Heihe river basin show that, the model can be used to effectively reveal the temporal and spatial variations of hydrological cycle and water budgets components as well as energy cycle components. The results of applying the model to predict the water budgets under the future land surface change show that, due to the construction of conservation forest in the upper reach basin, although the evapotranspiration from interception increases, the soil evaporation reduces at the same time, therefore the total evapotranspiration does not increase obviously; the runoff outflow slightly decreases, while the storage variable of soil moisture and groundwater slightly increase at the same time. The measure of changing the farmland to animal husbandry land in the middle reach basin has obvious effects on decreasing evapotranspiration, increasing the discharge at Zhengyixia as well as decreasing the storage variable deficit.

Acknowledgement. The research got financial supports from the National Scientific Foundation of China (NSFC) Projects (50721006, 50779074), the National 973 Program of

China (2006CB403404), and the National Science and Technology Supporting Plan of China (2001BA610A02, 2006BAB06B06).

References

Abbott, M. B., Bathurst, J. C., Cunge, J. A., O'Connell, P. E., and Rasmussen, J.: An introduction to the European hydrological system – Systeme Hydrologique Europeen, "SHE", 2: Structure of a physically-based distributed modelling system [J], J. Hydrol., 87, 61–77, 1986.

Avissar, R. and Pielke R. A.: A parameterization of heterogeneous land-surface for atmospheric numerical models and its impact on regional meteorology. Mon. Wea. Rev., 117, 2113–2136, 1989.

Cao, J., Xie, Y., Chen, Z., and Zhang, G.: Preliminary research on the seepage and transportation of irrigation water in the plain of main stream region of Heihe river Gansu province, Hydrogeol. Eng. Geol., 4, 1–4, 2000.

CAS-CAREERI (Chinese Academy of Sciences, Cold and Arid Regions Environment and Engineering Research Institute): Research Report on the Water Resources Change in the Mountain Region of the Heihe River Basin, the Hexi Corridor of China, 2000.

Cong, Z., Lei, Z., Hu, H., and Yang, S.: Study on coupling between winter wheat growth and water-heat transfer in soil-plant-atmosphere continuum I: Model, J. Hydr. Eng., 36(5), 575–580, 2005.

Dickinson, R. E.: Modelling evapotranspiration for three-dimensional global climate sensitivity. Geophysical Monograph 29. Washington, DC: American Geophysical Union, 58–72, 1984.

Haverkamp, R., Vauclin, M., Touma, J., and Wierenga, P. J., Vauchad, G.: A comparison of numerical simulation models for one-dimensional infiltration, J. Soil Sci. Soc. Am., 41, 285–293, 1977.

Hu, Z. and Islam, S.: Prediction of ground surface temperature and soil moisture content by the force-restore method, Water Resour. Res., 31(10), 2531–2539, 1995.

Huang, Q. and Zhang, W.: Improvement and application of GIS-based distributed SWAT hydrological modeling on high altitude, cold, semi-arid catchment of Heihe river basin, China, J. Nanjing Forest, University (Natural Sciences Edition), 28(2), 22–26, 2004.

Jia, Y. and Tamai, N.: Modeling infiltration into a multi-layered soil during an unsteady rain, Ann. J. Hydr. Eng., JSCE, 41, 31–36, 1997.

Jia, Y., Ni, G., Kawahara, Y., and Suetsugi, T.: Development of WEP model and its application to an urban watershed, Hydrol. Process., 15(11), 2175–2194, 2001.
Jia, Y., Ni, G., Kawahara, Y., and Suetsugi, T.: Development of WEP model and its application to an urban watershed, Hydrol. Process., 15, 2175–2194, 2001.
Jia, Y. and Wang, H.: Progress and perspective of distributed hydrological models, Adv. Water Sci., 14, 118–123, 2003.
Jia, Y.: The development and application of WEP model, Adv. Water Sci., 14, 50–56, 2003.
Kang, E., Cheng, G., Lan, Y., et al.: Application of a conceptual hydrological model in the runoff forecast of a mountainous watershed, Adv. Water Sci., 17(1), 18–26, 2002.
Kawamata, K.: Development of a 3-D urban climate model for an analysis of thermal environment (in Japanese), Master Degree thesis submitted to the Univ. of Tokyo, 1994.
Kondo, J.: Meteorology of Water Environment (in japanese). Asakura Press: Tokyo, 348 p., 1994.
Mein R. G. and Larson C. L.: Modeling infiltration during a steady rain, Water Resour. Res., 9(2), 384–394, 1973.
Monteith, J. L.: Principles of Environmental Physics. Edward Arnold, 1973.
Moor, I. D. and Eigel, J. D.: Infiltration into two-layered soil profiles, Trans. ASAE, 24, 1496–1503, 1981.
Mualem, Y.: Hydraulic conductivity of unsaturated porous media: generalized macroscopic approach, Water Resour. Res., 14(2), 325–334, 1978.
Noilhan, J. and Planton, S. A.: Simple parameterization of land surface processes for meteorological models, Mon. Wea. Res., 117, 536–549, 1989.
Shimazaki, H.: A comprehensive approach of deducing hourly solar radiation from sunshine hour data of AMeDAS (in Japanese), Proc. of Annual Conference of JSHWR, 96, 108–109, 1996.
Wang, W., Wang, Q., Zhang, J., and Wang, Z.: Soil hydraulic properties and correlation in Qingwangchuan area of Gansu province, J. Soil Water Cons., 16(3), 110–113, 2002.
Wu, Q., Xu, J., Zhang, Z., and Ma, Z.: Coupled modeling of surface water-groundwater system II: Application, J. Hydr. Eng., 36(6), 754–758, 2005.
Xia, J., Wang, G., Lv, A. et al.: A research on distributed time variant gain modeling, Acta Geo. Sinica, 58(5), 789–796, 2003.
Zhang, G., Nie, Z., Zhang, C., and Shen, J.: Mechanism and characteristics of groundwater replenishment variation in middle reaches of Heihe River basin, J. Hydr. Eng., 36(6), 715–

720, 2005.
Zhu, Y. and Wu, Y.: Determination on water movement parameters in populus euphratica roots of Ejina county – by Richard Equation and atmospheric data, Hydrology, 22(1), 3–5, 2002.
Zaradny, H.: In Groundwater flow in saturated and unsaturated soil, Balkema press, 350 p., 1993.

Table 1. Soil moisture characteristics parameters.

Parameters	Sand	Loam	Clay
Saturated moisture content θ_s	0.4	0.422	0.394
Residual moisture content θ_r	0.077	0.104	0.120
Single molecule moisture content θ_m	0.015	0.05	0.111
Field capacity θ_f	0.174	0.321	0.374
Saturated hydraulic conductivity k_s (m/s)	2.5E-5	7E-6	2E-6
Parameter α for Havercamp equation	1.7E10	6451	6.58E6
Parameter β for Havercamp equation	16.95	5.56	9.00
Parameter n for Mualem equation	3.37	3.97	4.38

Table 2. Simulation results of monthly discharge process at Yingluoxia station.

	Observed annual average discharge (10^8 m^3)	Simulated annual average discharge (10^8 m^3)	Relative error	Nash-Sutcliffe efficiency coefficient	Correlation coefficient
Calibration period (1996–2000)	16.85	16.82	–0.2%	0.85	0.96
Validation period 1 (1982–1995)	16.19	16.21	0.1%	0.89	0.96
Validation period 2 (2001–2002)	14.61	14.10	–3.5%	0.91	0.95

HESSD
6, 2189–2246, 2009

Table 3. Simulation results of daily discharge process at Yingluoxia station.

	Observed annual average discharge (10^8 m^3)	Simulated annual average discharge (10^8 m^3)	Relative error	Nash-Sutcliffe efficiency coefficient	Correlation coefficient
Calibration period (1996–2000)	16.85	16.82	–0.2%	0.60	0.88
Validation period 1 (1990–1995)	14.77	14.72	–0.4%	0.65	0.89
Validation period 2 (2001–2002)	14.61	14.10	–3.5%	0.78	0.89

HESSD
6, 2189–2246, 2009

Table 4. Impacts of conservation forest construction on water budgets in the upper reach (Unit: mm/year).

Land surface condition	Precipitation	Evapotranspiration from interception	Soil evaporation	Total evapotranspiration	Runoff outflow	Storage variable
Current level	397.6	122.9	135.4	258.3	153.7	–14.4
Conservation forest construction	397.6	129.6	129.5	259.1	152.2	–13.7

HESSD
6, 2189–2246, 2009

Table 5. Impacts of changing farmland to animal husbandry land on water budgets in the middle reach basin (Unit: mm/year).

Land surface condition	Precipitation	Inflow (Yingluoxia and Liyuanbu)	Evapotranspiration	Outflow (Zhengyixia)	Storage variable
Current level	193.4	92.1	282.7	41.3	–38.5
Changing farmland to animal husbandry land	193.4	92.1	240.1	52.8	–7.4

HESSD
6, 2189–2246, 2009

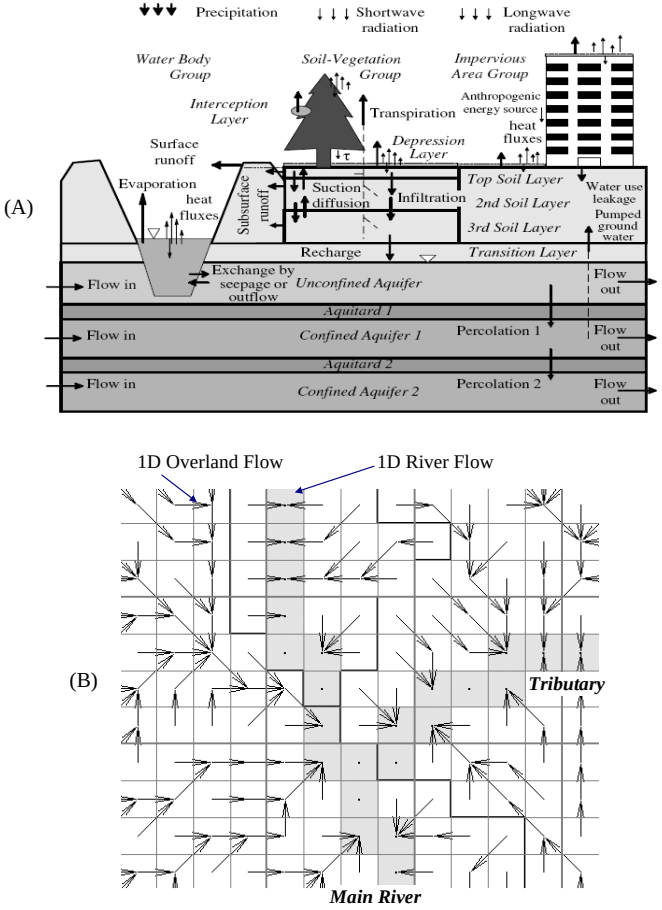

Fig. 1. Structure of WEP model: **(a)** vertical structure within a grid cell and **(b)** horizontal structure.

HESSD
6, 2189–2246, 2009

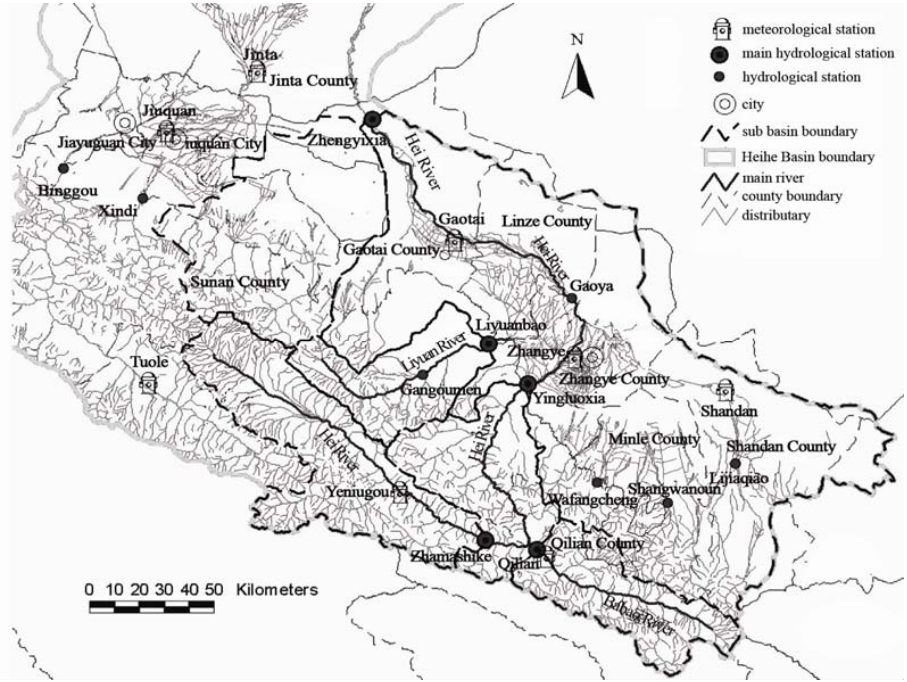

Fig. 2. Main rivers and hydro-meteorological stations in the upper and middle reach basin.

HESSD
6, 2189–2246, 2009

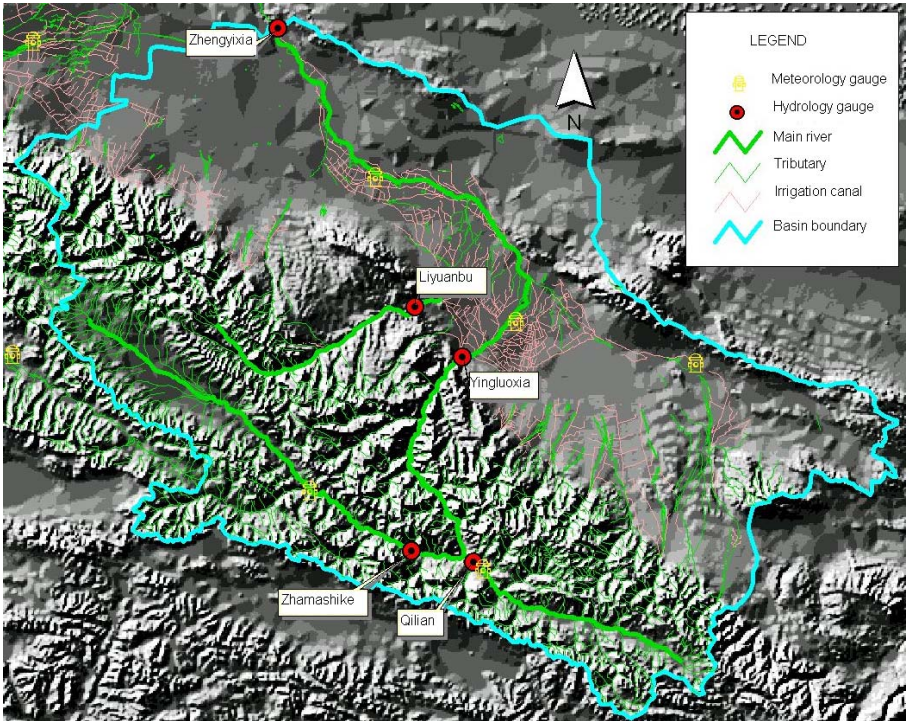

Fig. 3. Topography in the upper and middle reach basin.

HESSD
6, 2189–2246, 2009

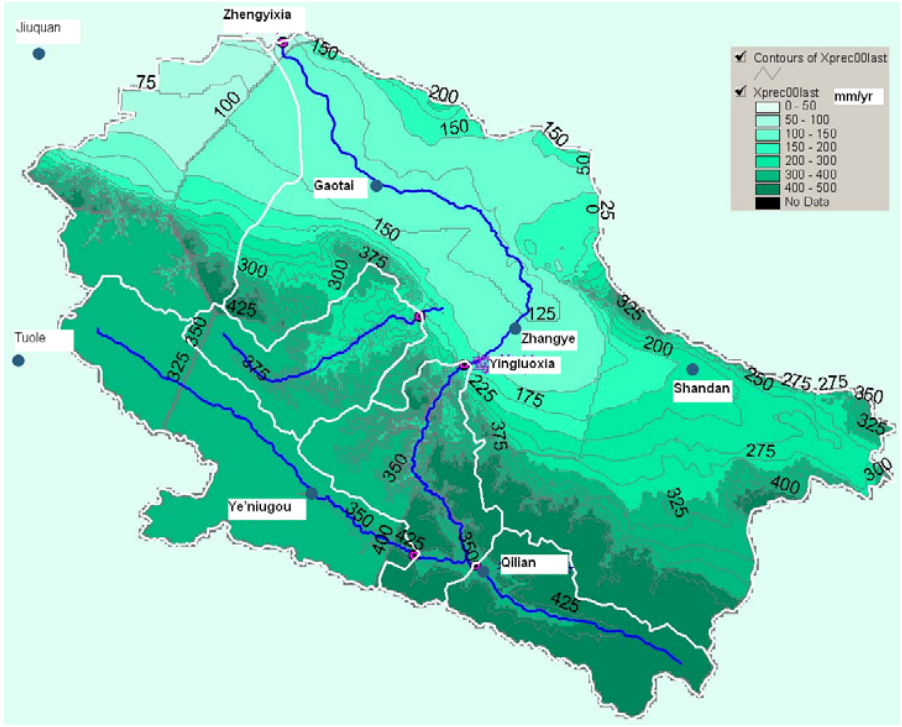

Fig. 4. Distribution of total precipitation in 2000 in the upper and middle reach basin.

HESSD
6, 2189–2246, 2009

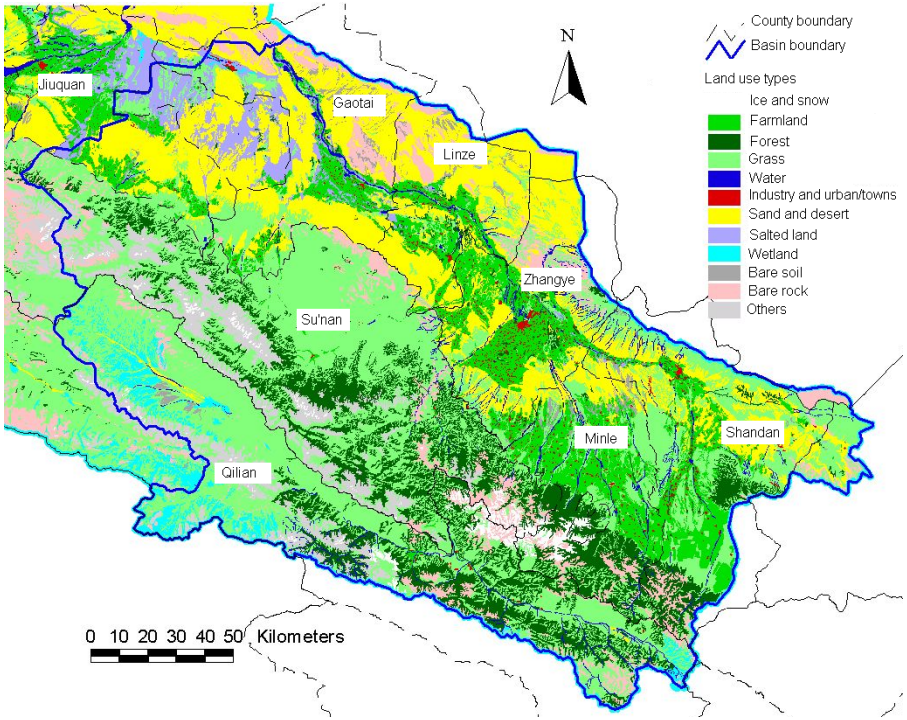

Fig. 5. Land use (2000) distribution in the upper and middle reach basin.

HESSD
6, 2189–2246, 2009

(A) Calibration period

(B) Validation period 1

(C) Validation period 2

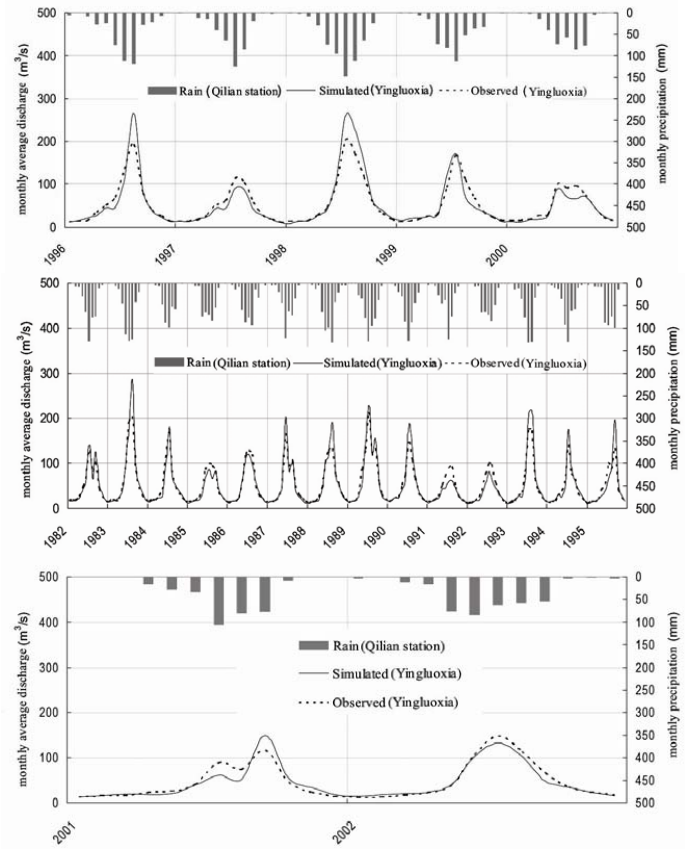

Fig. 6. Comparison of simulated results with observed values at Yingluoxia station.

HESSD
6, 2189–2246, 2009

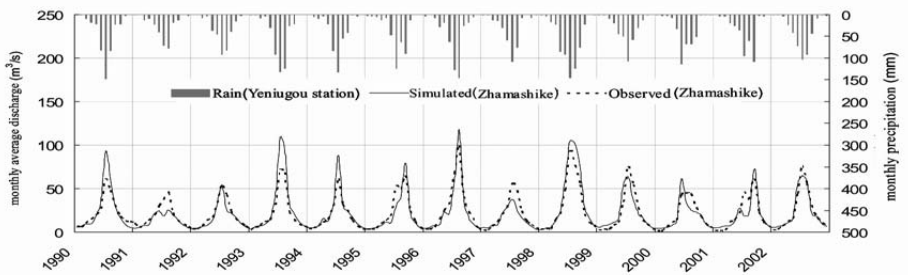

Fig. 7. Comparison of simulated results with observed values at Zhamashike station.

HESSD
6, 2189–2246, 2009

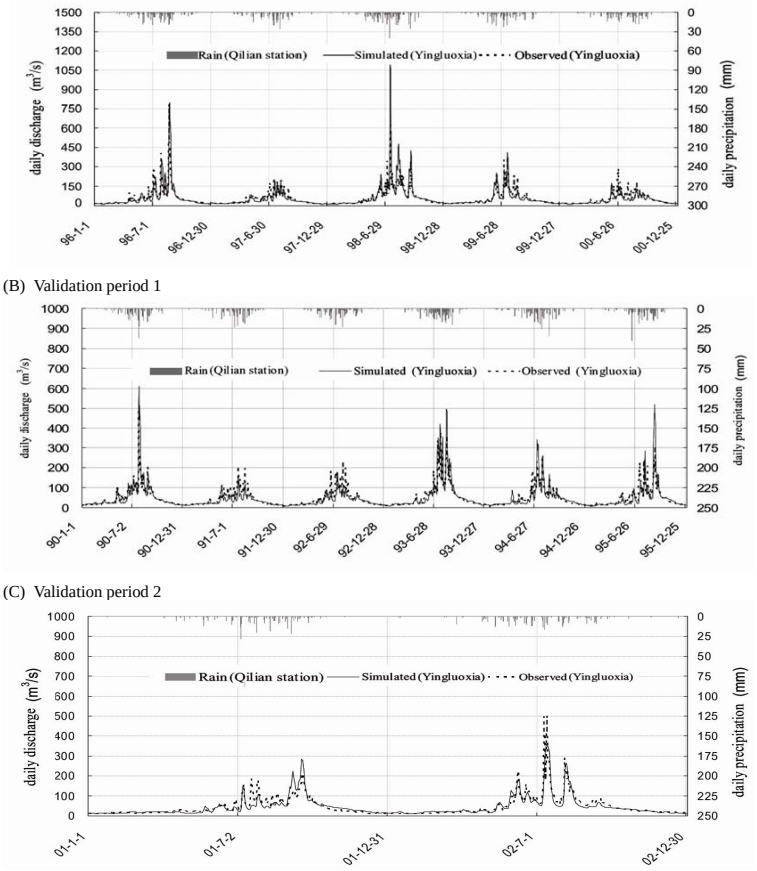

Fig. 8. Comparison of simulated results with observed values at Yingluoxia station.

HESSD
6, 2189–2246, 2009

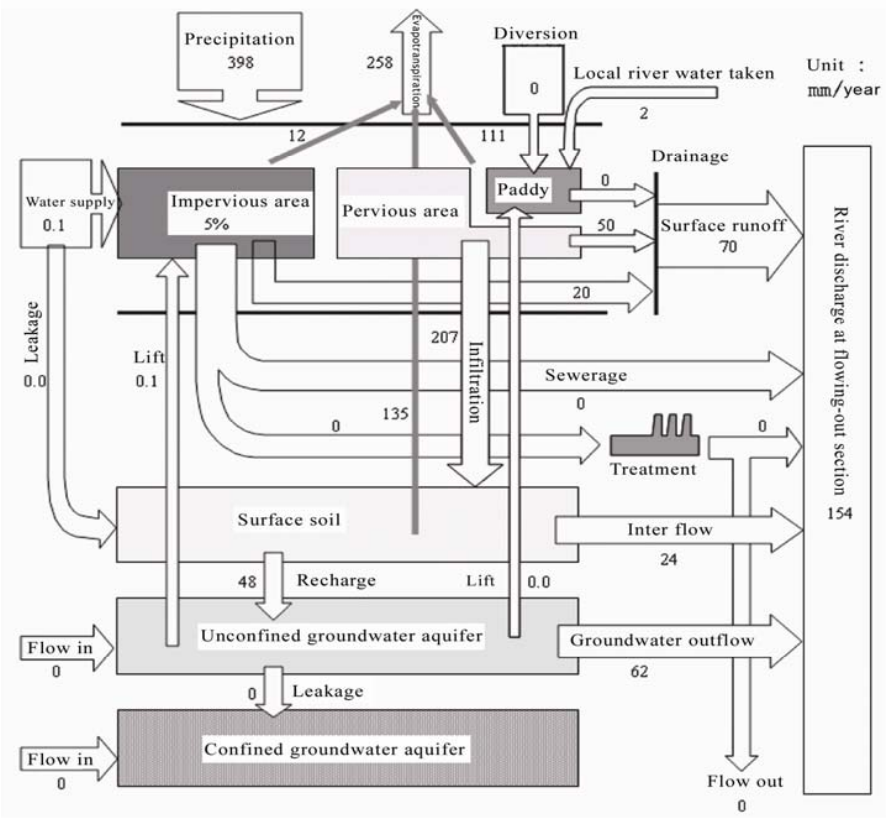

Fig. 9. Water budgets in the basin in 1999.

HESSD
6, 2189–2246, 2009

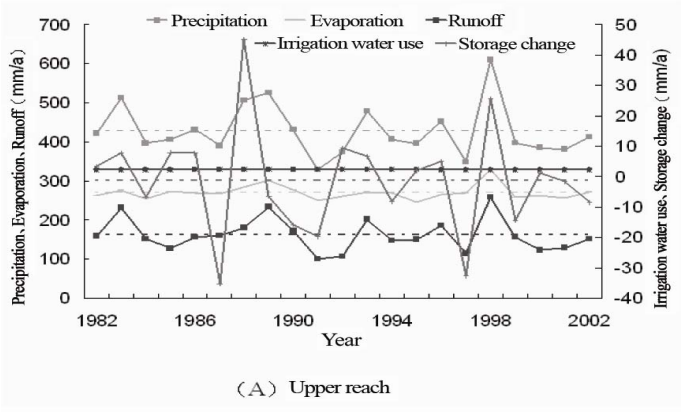

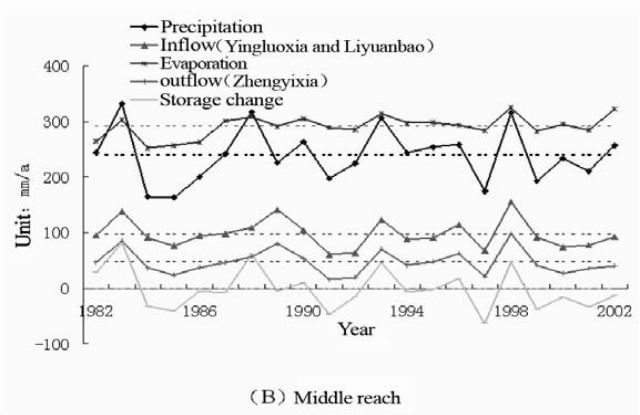

Fig. 10. Annual variations of hydrological cycle components in the upper and middle reach basin during 1982–2002.

HESSD
6, 2189–2246, 2009

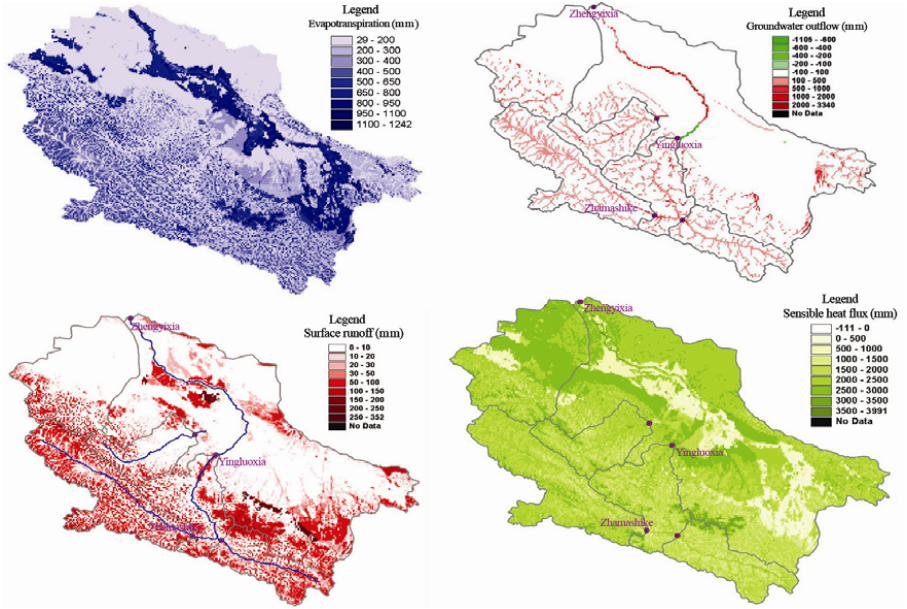

Fig. 11. Spatial variations of hydrological processes and sensible heat flux in the upper and middle reaches basin in 2000.

HESSD
6, 2189–2246, 2009

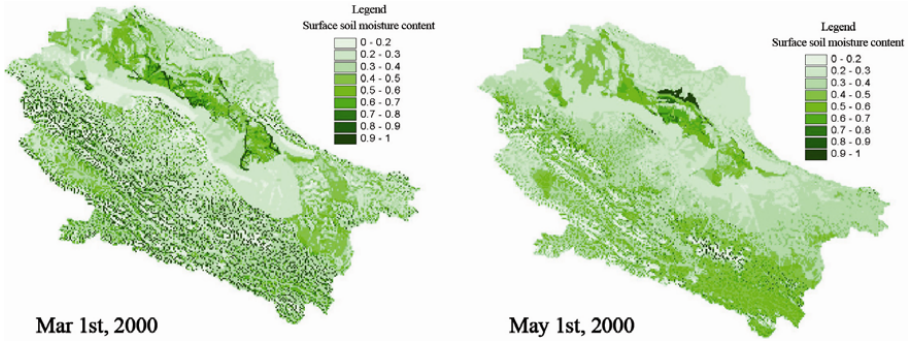

Fig. 12. Spatial variation of surface soil moisture.

HESSD
6, 2189–2246, 2009

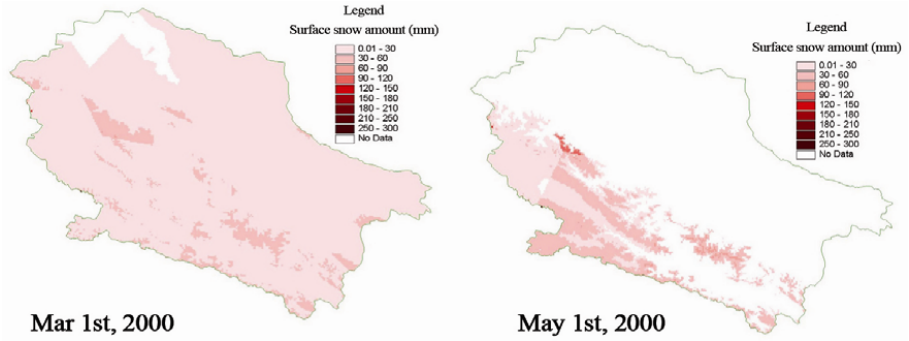

Fig. 13. Spatial variation of snow.

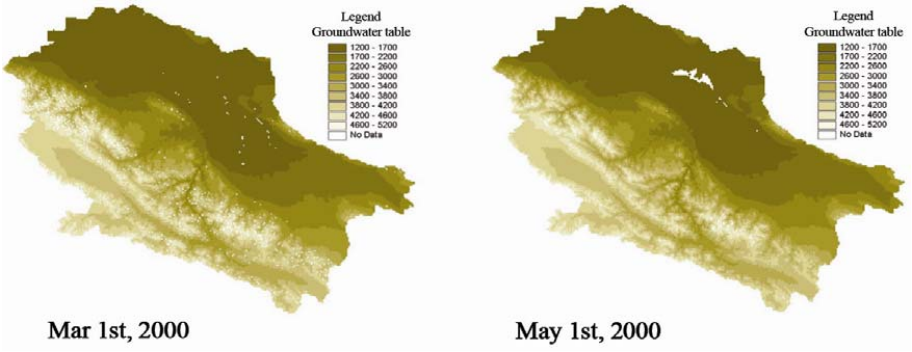

Fig. 14. Spatial variation of groundwater table.

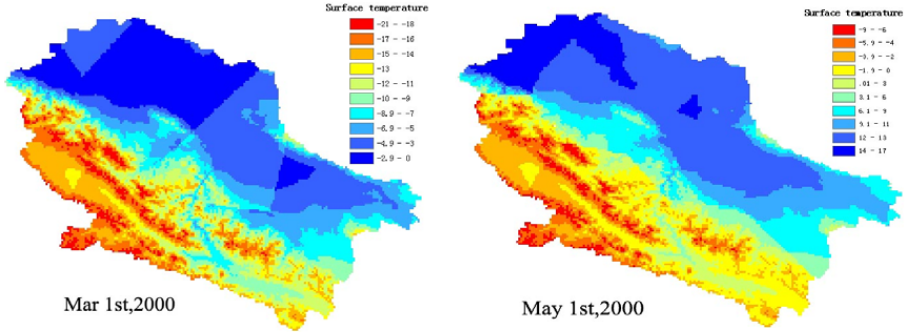

Fig. 15. Spatial variation of surface temperature.

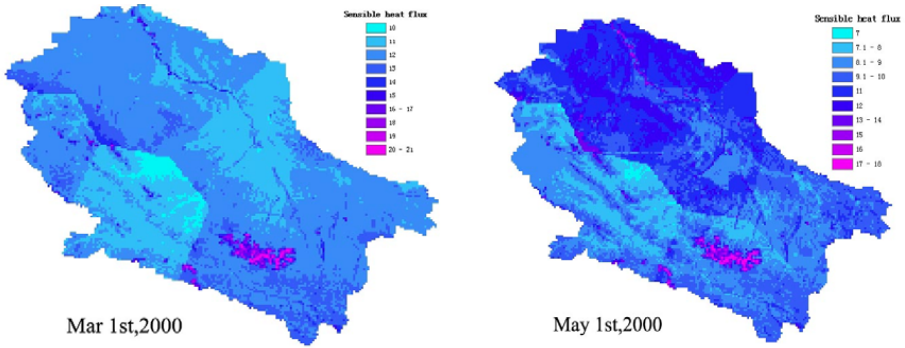

Fig. 16. Spatial variation of sensible heat flux.

HESSD
6, 2189–2246, 2009

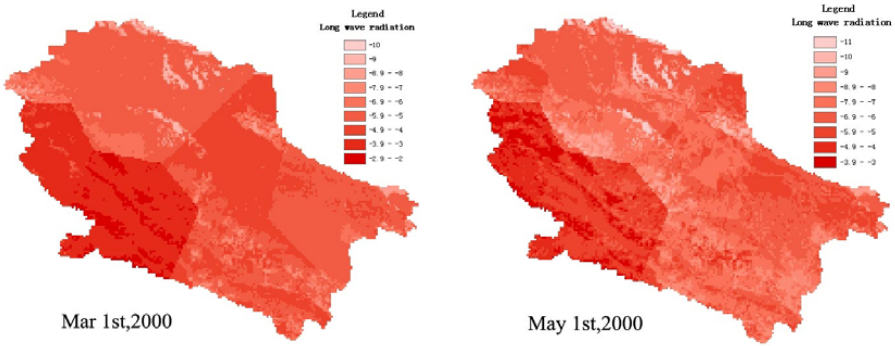

Fig. 17. Spatial variation of long-wave radiation.

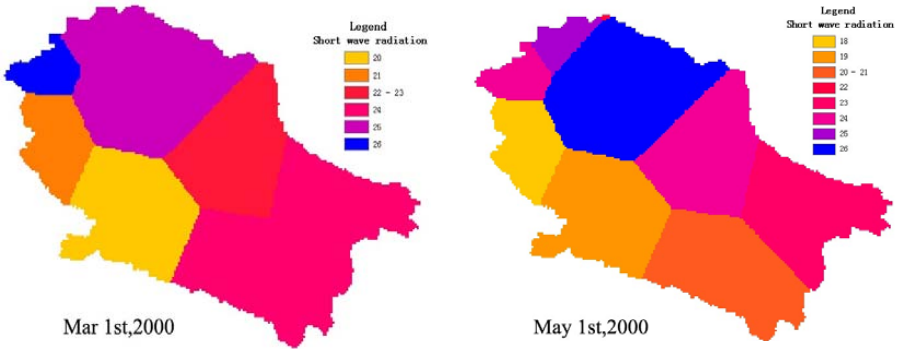

Fig. 18. Spatial variation of short-wave radiation.

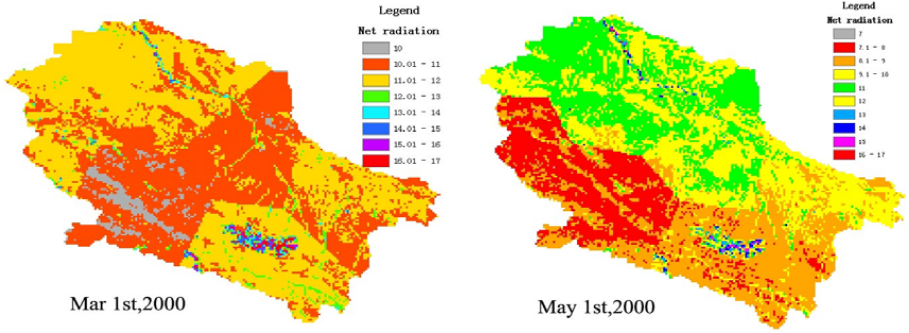

Fig. 19. Spatial variation of net radiation.

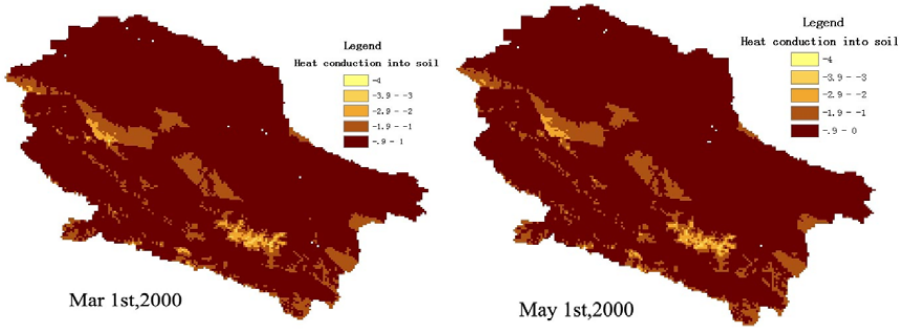

Fig. 20. Spatial variation of heat conduction into soil.

HESSD
6, 2189–2246, 2009